

# A canonical response of precipitation characteristics to global warming from CMIP5 models

William K.-M. Lau,<sup>1</sup> H.-T. Wu,<sup>2</sup> and K.-M. Kim<sup>3</sup>

Received 12 February 2013; revised 26 March 2013; accepted 26 March 2013; published 26 June 2013.

[1] In this study, we find from analyses of projections of 14 CMIP5 models a robust, canonical global response in rainfall characteristics to a warming climate. Under a scenario of 1% increase per year of CO<sub>2</sub> emission, the model ensemble projects globally more heavy precipitation ( $+7 \pm 2.4\%K^{-1}$ ), less moderate precipitation ( $-2.5 \pm 0.6\%K^{-1}$ ), more light precipitation ( $+1.8 \pm 1.3\%K^{-1}$ ), and increased length of dry (no-rain) periods ( $+4.7 \pm 2.1\%K^{-1}$ ). Regionally, a majority of the models project a consistent response with more heavy precipitation over climatologically wet regions of the deep tropics, especially the equatorial Pacific Ocean and the Asian monsoon regions, and more dry periods over the land areas of the subtropics and the tropical marginal convective zones. Our results suggest that increased CO<sub>2</sub> emissions induce a global adjustment in circulation and moisture availability manifested in basic changes in global precipitation characteristics, including increasing risks of severe floods and droughts in preferred geographic locations worldwide. **Citation:** Lau, W. K.-M., H.-T. Wu, and K.-M. Kim (2013), A canonical response of precipitation characteristics to global warming from CMIP5 models, *Geophys. Res. Lett.*, 40, 3163–3169, doi:10.1002/grl.50420.

## 1. Introduction

[2] One of the key findings of the Fourth Assessment Report (AR4) of the Intergovernmental Panel on Climate Change (IPCC) is that “*anthropogenic influences have contributed to intensification of extreme precipitation at the global scale*” [IPCC, 2007]. The AR4 also noted that while climate models generally project a global increase in rainfall, the projected rate of change and regional signals are highly uncertain due to coarse model resolution and inadequate model physics. In recent years, many record breaking heavy rain, and prolonged heat waves and drought events have been reported worldwide [Field *et al.*, 2012]. This is consistent with a growing body of contemporaneous studies suggesting that there is an increased risk of extreme rain events in a warmer climate [Allan *et al.*, 2010;

Groisman *et al.*, 2005; Lau and Wu, 2007, 2011; Liu *et al.*, 2012; Min *et al.*, 2011; O’Gorman and Schneider, 2009; Trenberth *et al.*, 2003; Trenberth 2011]. However, the regional distribution of the increased extreme rain and attribution of precipitation variability to specific climate forcing are still uncertain, and increasing the confidence of future projection of rainfall pattern remains a challenge [Kharin *et al.*, 2007; Sun *et al.*, 2012]. In preparation for the Fifth Assessment Report (AR5), IPCC has organized the Coupled Model Intercomparison Project Phase 5 (CMIP5), coordinating major international research institutions and groups to conduct climate projection experiments using state-of-the-art models with higher resolution and more realistic physics. The results presented in this paper are based on climate projection experiments from 14 CMIP5 models available at the time of this study. While the 14 models have diverse resolutions (Table S1 in the auxiliary material) and representations of physical, chemical, hydrological, and oceanic processes, they are subject to the same set of prescribed greenhouse gases (GHG) emission scenarios [Taylor *et al.*, 2012]. Here we assess CMIP5 model projections of global and regional rainfall response to GHG warming, specifically to increased CO<sub>2</sub> emissions. This study differs from previous global warming rainfall studies in that they were mostly focused on extreme rain, or on severe drought separately based on total rain, while we emphasize the changes in rainfall characteristics (types, intensity, and duration) and connections between extreme rain and drought events. We will examine rainfall changes not only in total rain, but also changes in the entire rainfall probability distribution function (PDF), including heavy, moderate, light, and no-rain events.

[3] We analyze the outputs of 14 CMIP5 models based on a 140 year experiment with a prescribed 1% per year increase in CO<sub>2</sub> emission. This rate of CO<sub>2</sub> increase is comparable to that prescribed for the RCP8.5, a relatively conservative business-as-usual scenario [Riahi *et al.*, 2011], except the latter includes also changes in other GHG and aerosols, besides CO<sub>2</sub>. A 27-year period at the beginning of the integration is used as the control to compute rainfall and temperature statistics, and to compare with climatology (1979–2005) of rainfall data from the Global Precipitation Climatology Project (GPCP). Two similar 27-year periods in the experiment that correspond approximately to a doubling of CO<sub>2</sub> emissions (DCO2) and a tripling of CO<sub>2</sub> emissions (TCO2) compared to the control are chosen respectively to compute the same statistics (for details, see section S1 in the auxiliary material). The rainfall response to global warming is defined as the difference in the statistics between the control and DCO2, and TCO2, respectively. Since the responses based on DCO2 and TCO2 are similar, except with stronger and more

All supporting information may be found in the online version of this article.

<sup>1</sup>Laboratory for Atmospheres, NASA Goddard Space Flight Center, Greenbelt, Maryland, USA.

<sup>2</sup>Science Systems and Applications, Inc., Lanham, Maryland, USA.

<sup>3</sup>Goddard Earth Science Technology & Research, Morgan State University, Baltimore, Maryland, USA.

Corresponding author: W. K.-M. Lau, Earth Science Division, Atmospheres, Code 613, Building 33, Rm C121, NASA Goddard Space Flight Center, Greenbelt, MD 20771, USA. (William.K.Lau@nasa.gov)

©2013. American Geophysical Union. All Rights Reserved.  
0094-8276/13/10.1002/grl.50420

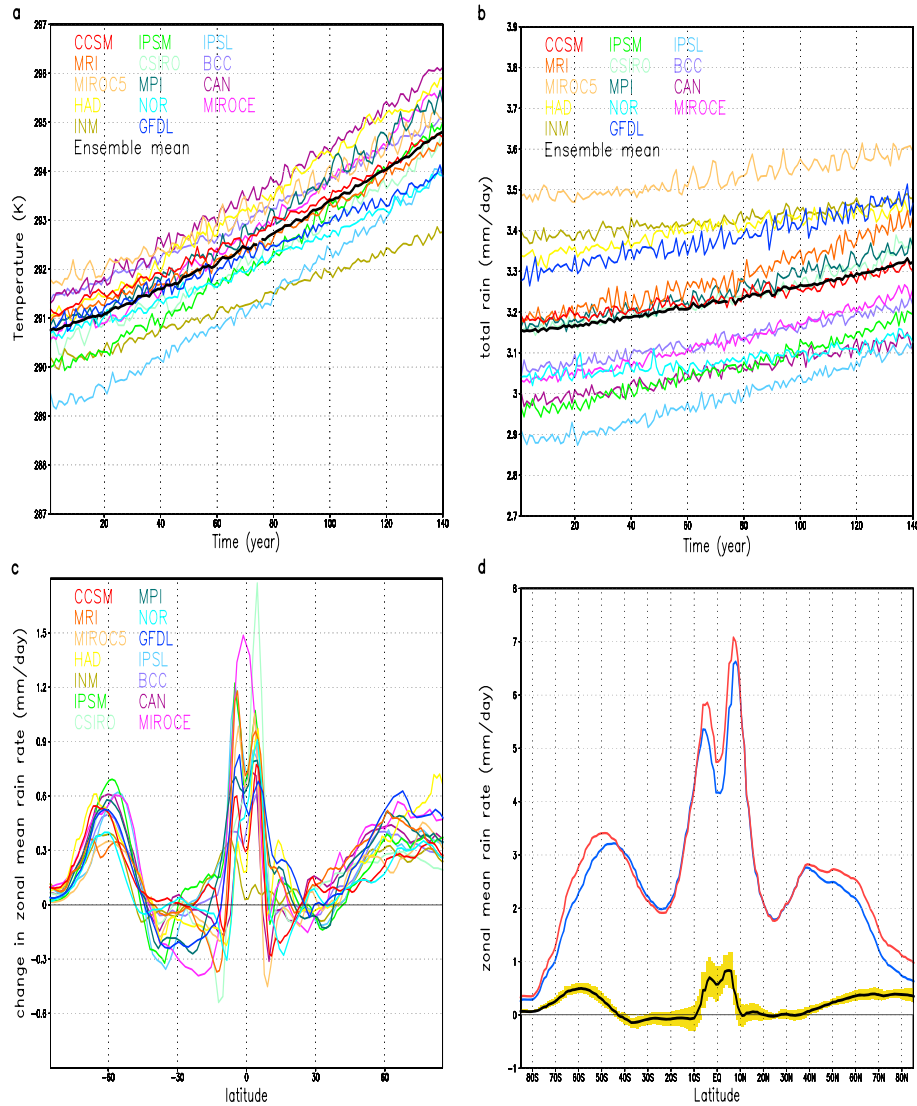


**Figure 1.** CMIP5 projections of changes in global mean surface temperature and precipitation induced by increased CO<sub>2</sub> emissions. Time series of global (60°S–60°N) annual mean (a) surface temperature and (b) rainfall from year 1 to year 140, based on experiment with 1% increase CO<sub>2</sub> emissions per year; (c) the difference in the zonal mean rain rate of the control and TCO2 for each of the 14 CMIP5 models as a function of latitude; and (d) the ensemble averaged zonal mean rain rates of the control (blue) and TCO2 (red), the ensemble-mean response (TCO2 minus control, black) and the inter-model 1– $\sigma$  deviation (yellow shading).

robust signal in the latter, unless otherwise stated, results presented are for TCO2.

## 2. Model Rainfall Climatology

[4] The rainfall PDFs and cumulative PDFs (CPDFs) for rainfall occurrences and amount, as well as climatological global and zonal mean rainfall distributions for the model ensemble mean, have been computed and found to be in reasonable agreement with GPCP and Tropical Rainfall Measuring Mission (TRMM) observations (see section S2 and Figure S1 in the auxiliary material).

[5] To facilitate discussion regarding rainfall characteristics in this work, we define, based on the ensemble model PDF, three major rain types: light rain (LR), moderate rain (MR), and heavy rain (HR) respectively as those with monthly mean rain rate below the 20th percentile ( $<0.3$  mm/day), between

the 40th–70th percentile (0.9–2.4 mm/day), and above the 98.5% percentile ( $>9$  mm/day). An extremely heavy rain (EHR) type defined at the 99.9th percentile ( $>24$  mm day<sup>−1</sup>) will also be referred to, as appropriate. The geographic distributions of the three rain types agree quite well between the model ensemble mean and GPCP (Figure S2 and section S2 in the auxiliary material), with HR most dominant over the deep convection zone of the tropics, and monsoon regions MR over mid-latitude storm tracks over the continents and the Southern Oceans, and LR over the desert and semiarid zones, and the subtropical stratocumulus region off the west coast of the Americas and South Africa. Previous studies [Lau and Wu 2007; 2011] have found that based on a similar classification, LR, MR, and HR can be identified with rainfall subsystems dominated by warm-rain/low clouds, mixed-phase/congestus, and ice-phase rain/deep convection respectively in the tropics. Hence, to a first-order

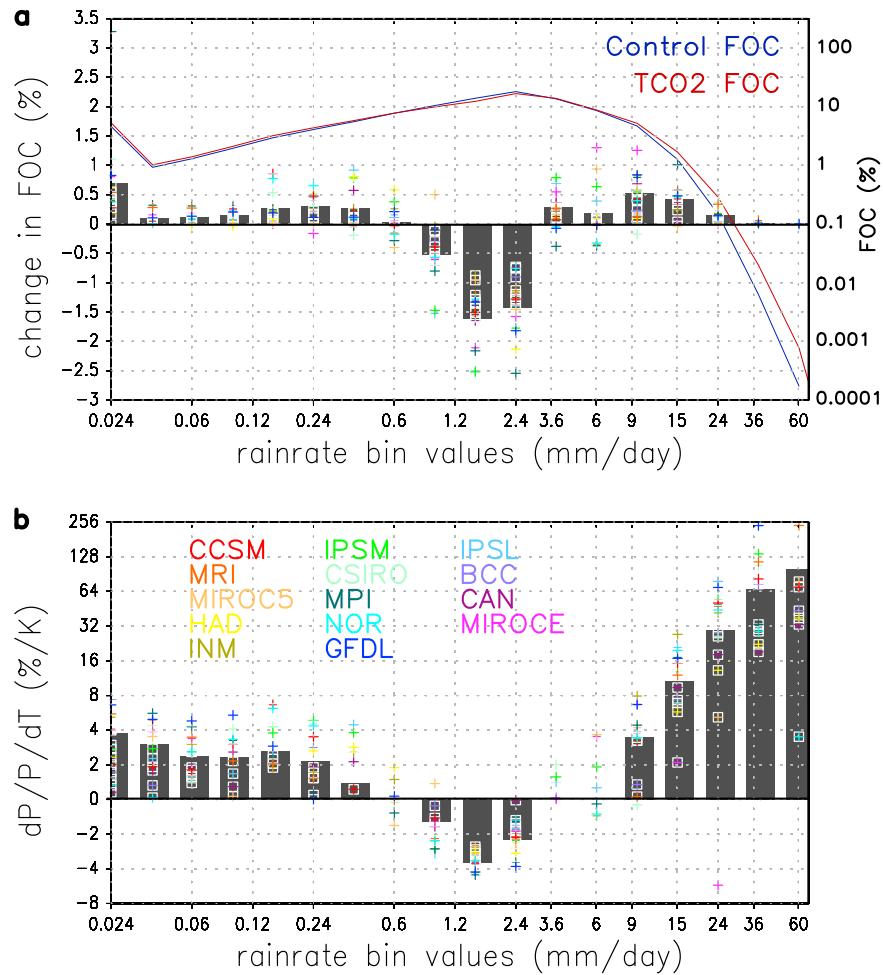


**Figure 2.** Response in global (60°S–60°N) annual mean precipitation for TCO2 as a function of rain rate. (a) Change in the frequency of occurrence (FOC) and (b) sensitivity of precipitation amount to temperature change. Response of each of the 14 CMIP5 models is denoted by different color marks, and the model ensemble mean is denoted by the bar chart. Also shown in Figure 2a are the ensemble mean FOC of the control and TCO2 (solid curves), in logarithmic scale.

approximation, the aforementioned rain types provide a natural separation of rainfall subsystems associated with major climatic regimes. It should also be pointed out that the rain type definition used here is based on global scaling with monthly mean data to facilitate a global narrative. Obviously, this definition has limitations and cannot be used for detailed regional or singular extreme event applications, for which a local relative scaling, with daily or hourly rainfall should be used.

### 3. Response in Total Rainfall

[6] All models show a clear increase in global (60°S–60°N) mean temperature due to increased CO<sub>2</sub> emissions, with a rate of 0.2–0.36 K decade<sup>−1</sup> among models, and an ensemble mean of 0.26 K decade<sup>−1</sup> (Figure 1a). Similarly, all models exhibit a clear upward trend in the annual global mean precipitation, with an ensemble mean rate of 0.012 mm day<sup>−1</sup>decade<sup>−1</sup> or 0.38% decade<sup>−1</sup> (Figure 1b). In the zonal mean, most models show increased rainfall in the deep tropics (10°S–10°N) and mid-to-high latitudes (Figure 1c). Reduced rainfall is found in the subtropics, more pronounced in the Southern Hemisphere (SH) than the Northern Hemisphere (NH), with large variability

among models. The model ensemble response (Figure 1d) shows three distinct zones of rainfall increase: 10°S–10°N, south of 45°S, and north of 40°N; a wide rainfall-reduction zone near 10°S–40°S, and a rainfall-neutral zone near 20°N–40°N. These signals are highly significant (>95–99% c.l.) based on a Student's *t*-test, in the deep tropics and high (>45°) latitudes, but less so in the subtropics. Additional analyses of zonal mean profiles over selected longitudinal sectors (section S3 and Figure S3 in the auxiliary material) show rainfall reduction in the NH subtropics over North America, and the Europe-Africa sectors, but enhancement over the subtropical central Pacific and Asian monsoon sectors. These regional rainfall anomalies compensate to produce in the zonal mean a near neutral zone over the NH subtropics (Figure 1d). The rainfall anomalies are consistent with observations of a narrowing of the deep convection zone in the tropics and a widening of the subtropical belt in recent decades [Seidel *et al.*, 2008; Hu and Fu, 2007; Zhou *et al.*, 2011].

[7] Globally, rainfall increases by 4.5%, with a sensitivity ( $dP/P/dT$ ) of 1.4% K<sup>−1</sup> (Table S2 in the auxiliary material), substantially lower than the 7% K<sup>−1</sup> increase in saturated water vapor governed by the Clausius-Clapeyron relation, consistent with previous findings [Held and Soden, 2006;

**Table 1.** Sensitivity ( $dP/P/dT$ ) of the Ensemble-Mean Global (60°S to 60°N) Precipitation to CO<sub>2</sub> Induced Warming for Different Rain Types<sup>a</sup>

Rain types	ALL	Extremely Heavy (EH)	Heavy (HR)	Moderate (MR)	Light (LR)
DCO2	$1.31 \pm 0.38$	$26.8 \pm 19.2$	$7.25 \pm 2.32$	$-2.51 \pm 0.62$	$1.86 \pm 1.30$
TCO2	$1.35 \pm 0.38$	$32.1 \pm 26.6$	$6.98 \pm 2.40$	$-2.51 \pm 0.56$	$1.81 \pm 1.27$

<sup>a</sup>Uncertainties are estimated from inter-model standard deviation for different rain types. Units are in % K<sup>-1</sup>.

Andrews et al., 2010; Frieler et al., 2011; Vecchi et al., 2006; Giorgi et al., 2011]. The highest sensitivity  $+6.3\% \text{ K}^{-1}$  is found over southern mid-to-high-latitudes (50–80°S). The northern mid-to-high-latitudes (50–80°N) and the equatorial region (10°S–10°N) also show high ( $+3\% \text{ K}^{-1}$ ) sensitivity. Negative sensitivity is found over the NH subtropics, SH subtropics, and mid-latitudes, suggesting the importance of large-scale circulation forcing and dynamical feedback [Lau and Wu, 2011; Chou et al., 2012].

#### 4. Changes in Rainfall Characteristics

[8] The changes in rainfall characteristics are analyzed based on the monthly PDFs of rainfall frequency of occurrences (FOC) (Figure 2a) and amount (Figure 2b). The ensemble-mean FOC (Figure 2a, line graphs in logarithmic scale) clearly show that there is a tendency for increase in HR events

globally due to CO<sub>2</sub> warming. However, the logarithmic scale in the mean FOC plot masks changes in lower rain rates. For a different perspective, the FOC difference plot (Figure 2a, bar chart) displays a consistent and robust model response, i.e., more HR, less MR, and more LR. When the rainfall sensitivity is plotted as a function of rain types, a systematic, canonical pattern in response to CO<sub>2</sub> warming is evident, i.e., *higher positive sensitivity for increasingly heavy rain, negative sensitivity for moderate rain, and positive sensitivity for light rain* (Figure 2b). The sensitivity is quite high ( $4\text{--}10\% \text{ K}^{-1}$ ) for HR bins ( $9\text{--}15 \text{ mm day}^{-1}$ ), and increases dramatically ( $30\text{--}100\% \text{ K}^{-1}$ ) for EHR bins ( $> 24 \text{ mm day}^{-1}$ ). For MR and LR bins, the sensitivity is negative  $2\text{--}4\% \text{ K}^{-1}$ , and positive  $1\text{--}4\% \text{ K}^{-1}$ , respectively. Analyses of changes of rainfall PDFs over land, ocean separately, and for different latitudinal zones (section S4 and Figure S4 in the auxiliary material) show that

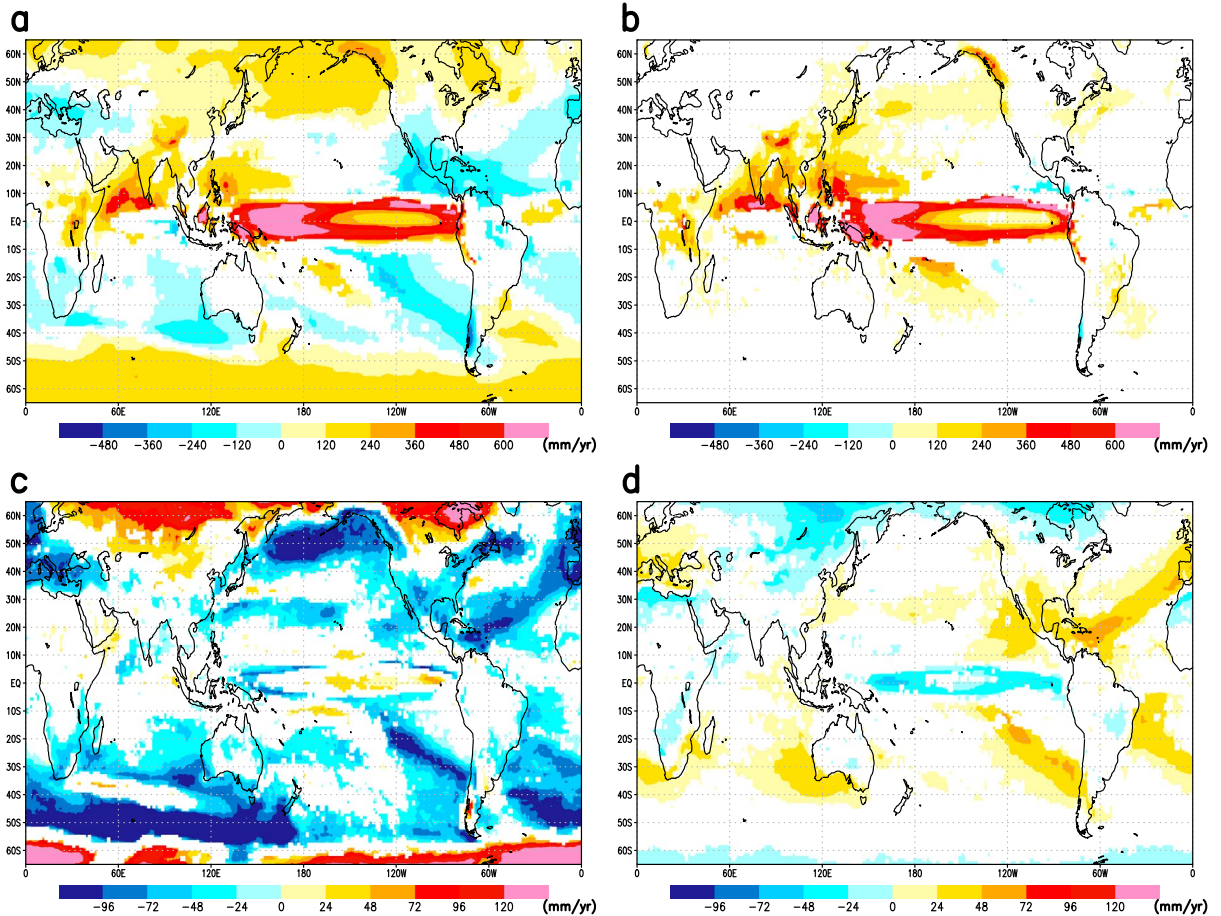


**Figure 3.** Geographic distribution of the model ensemble-mean response in rain amount for TCO2. Changes in ensemble-mean annual accumulation (mm/year) for (a) total rain, (b) heavy rain, (c) moderate rain, and (d) light rain. Only regions with high consistency, i.e., responses of 10 or more out of the 14 CMIP5 models of the same sign, are shown. All model outputs are interpolated to a common grid resolution ( $1.125^\circ$  longitude  $\times$   $1.07^\circ$  latitude;  $320 \times 192$  arrays).



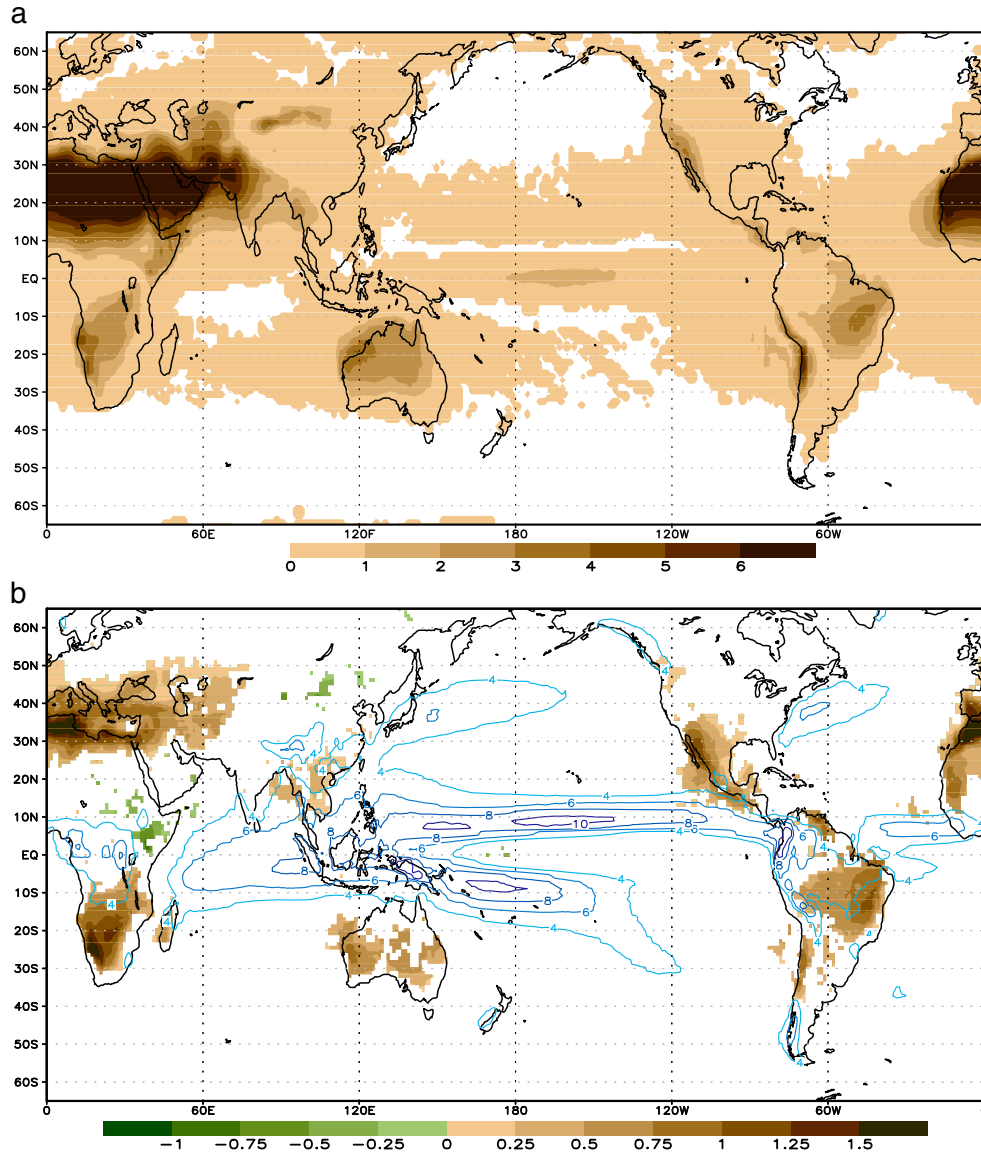


**Figure 4.** Geographic distribution of the model ensemble annual dry-month duration (a) climatology, and (b) changes due to TCO<sub>2</sub> scenario. Units are in number of dry months per year. Also superimposed in Fig. 4b is the ensemble-mean precipitation (in mm/day) for the control period in contour lines. As in Figure 3, only regions with high consistency are shown in Figure 4b.

the same canonical rainfall redistribution pattern is captured, provided sufficiently large domains are chosen. The canonical rainfall distribution in response to global warming is similar to that shown in a CMIP3 study over tropical land by *Lintner et al.* [2012]. The rainfall sensitivities remain approximately constant for total rain, and for LR and MR, respectively in DCO<sub>2</sub> and TCO<sub>2</sub> (Table 1), indicating that the overall rainfall response may have reached quasi-steady state under both scenarios. However, for heavy rain, the sensitivity is still evolving, with slightly reduced magnitude averaged for HR but increased for averaged EHR from 27% K<sup>-1</sup> to 32% K<sup>-1</sup> between the two scenarios. We further note that the sensitivity of the most extreme rain events (rain rate > 60 mm/day) is more than double (from 46% to 102% K<sup>-1</sup>) from DCO<sub>2</sub> to TCO<sub>2</sub> (compare Figure S5 in the auxiliary material and Figure 2). These results suggest that the canonical rainfall response to CO<sub>2</sub> warming is highly nonlinear and scale selective, with increasing sensitivity

in the most extremely heavy rain events as CO<sub>2</sub> emissions increase.

## 5. Geographic Distributions

[9] Geographic distributions are shown for the ensemble mean response for total rain, HR, MR, and LR, respectively (Figure 3). Here to emphasize model consistency, a grid-point ensemble value is displayed only if 10 or more models show the same sign of response. There is a large increase in total rain, most pronounced in climatologically wet regions of the tropics, especially over the equatorial western Pacific and the Asian monsoon regions including the northern Indian Ocean, South and Southeast Asia (Figure 3a). Rainfall is also moderately increased over the extratropics of both hemispheres poleward of 50° latitude. A general reduction of rainfall is found in the climatologically dry subtropical oceans, as well as in land regions of Central America and southwestern US, southern Europe/Mediterranean,

and South Africa. The CMIP5 projected changes in total rain shown in Figure 3a are consistent with the CMIP3 projected changes shown in the AR4 of IPCC (see IPCC [2007], Figure 10.12a). Our analyses further indicate, as shown in Figure 3b, that most of the increased rainfall in the deep tropics is contributed by HR. Notably, very few regions experience a reduction in HR anywhere in the globe. This is akin to the outcome of throwing a loaded dice with heavy odds in favor of increased HR events due to global warming.

[10] In contrast to HR, there is an overall reduction in MR over extensive regions in the subtropical and mid-latitude oceans (Figure 3c). Interestingly, significant increase of MR is found over high latitude land regions of North America and Eurasia, and the high latitude of the Southern Oceans ( $>50^{\circ}\text{S}$ ). It can also be seen that the anomalous dry regions over southwestern US, and southern Europe/Mediterranean noted previously (Figure 3a) may be attributed to changes in MR. These features may reflect the change in storm tracks in conjunction with the poleward migration of the jet stream induced by global warming [Yin, 2005; Scheff and Frierson, 2012]. Overall, LR (Figure 3d) has a distribution similar but with opposite signs to those of MR. The presence of many regions where the collocated rainfall responses have different signs in HR, MR, and/or LR may indicate change in the vertical structure of hydrometeors in clouds and rain systems over the regions [Lau and Wu, 2011].

[11] For drought assessment, we use the first rain bin ( $<0.024\text{ mm day}^{-1}$ ) to represent trace amount or no-rain events. The occurrence of such an event at each grid location will be hereafter referred to as a “dry month” for that location. Using this definition, dry months occur about 3–10% (ensemble mean = 5%) globally during the control period, but with negligible contribution to the rain amount (Figure S1b in the auxiliary material). The geographical distribution of climatologically dry months simulated by the ensemble model mean (Figure 4a) agrees reasonably well with that of the GPCP observation. Overall, the ensemble model mean over-estimates the aridity in subtropical land, but underestimates the dry oceanic stratocumulus zone off the west coast of Americas, and Africa (see section S6 and Figure S6 in the auxiliary material). From Figure 4a, pronounced no-rain periods can be identified with deserts and arid regions of North Africa /Middle East/Pakistan, northwestern China, and southwestern US in NH, and South Africa, northwestern Australia, coastal central America, and northeastern Brazil in SH.

[12] Under TCO2, the frequency of dry months in the ensemble mean increases by 16% at a rate of  $4.7\% \text{ K}^{-1}$  globally. Our results regarding the increase in HR and drought are consistent with the study of Giorgi *et al.* [2011] who show a projected increase ( $4.8\% \text{ K}^{-1}$ ) in the dry spell length as well as a general increase in hydroclimatic intensity from global model projections. Geographically, prolonged dry months occur predominantly over land areas in the subtropics or convective zones at the margins of climatological wet regions in both hemispheres (Figure 4b). Specifically, the model ensemble projects a pronounced increase in dry months over a long and narrow east-west zone extending from North Africa/Mediterranean/Southern Europe to Iran, and over southern Africa. Prolonged dry months are also found in southwestern US/Mexico region, and northeastern Brazil. Much weaker dry zones are found over Southeast Asia and southern Australia. The dry regions generally

coincide with reduced rainfall zones in the total rainfall distribution shown in Figure 3a. However, because of the positive-definite nature of rainfall, a prolonged period of no rain in climatologically dry regions will not always show up as a major anomaly in a rainfall map (Figure 3), but will be captured in a map of dry month distribution (Figure 4). Hence, regions shown in Figure 4b could be interpreted as those that have a higher risk of experiencing prolonged drought-like conditions under TCO2. Comparing with the model dry month climatology (Figure 4a), the model ensemble projects under TCO2, an expansion of the desert or arid-zones, both equatorward and poleward, over major continental land regions. Again, CMIP5 models project no spatially coherent *reduction* in dry months anywhere in the globe, analogous to the outcome of throwing a loaded dice with overwhelming odds in favor of prolonged droughts due to global warming.

## 6. Conclusions

[13] The IPCC CMIP5 models project a robust, canonical global response of rainfall characteristics to  $\text{CO}_2$  warming, featuring an increase in heavy rain, a reduction in moderate rain, and an increase in light rain occurrence and amount globally. For a scenario of 1%  $\text{CO}_2$  increase per year, the model ensemble mean projects at the time of approximately tripling of the  $\text{CO}_2$  emissions, the probability of occurring of extremely heavy rain (monthly mean  $>24\text{ mm/day}$ ) will increase globally by 100%–250%, moderate rain will decrease by 5%–10% and light rain will increase by 10%–15%. The increase in heavy rain is most pronounced in the equatorial central Pacific and the Asian monsoon regions. Moderate rain is reduced over extensive oceanic regions in the subtropics and extratropics, but increased over the extratropical land regions of North America, and Eurasia, and extratropical Southern Oceans. Light rain is mostly found to be inversely related to moderate rain locally, and with heavy rain in the central Pacific. The model ensemble also projects a significant global increase up to 16% more frequent in the occurrences of dry months (drought conditions), mostly over the subtropics as well as marginal convective zone in equatorial land regions, reflecting an expansion of the desert and arid zones. The most pronounced increased risks of prolonged drought are found over an east-west fetch spanning North Africa, Mediterranean Sea, southern Europe to Iran, and another one over southern Africa. A secondary region of increased risk of drought is found over Southwest US/Mexico, and northeastern Brazil. Weak signals of increased drought signals are found over southern Australia, and Indo-China. The propensity for prolonged dry months over tropical land regions and marginal tropical convective zones over large landmass is most likely due to the fact that land regions are moisture limited from evaporation while oceanic regions are not. As a result, in a competition of moisture availability, the land regions lose out. This also suggests the importance of land-atmosphere feedback through changes in soil moisture and surface evaporation in leading to severe droughts [Brubaker and Entekhabi, 1996; Sheffield and Wood, 2008]. Also note that the increased risk of drought due to global warming can be exacerbated in regions undergoing large deforestation or land use change [Lee *et al.*, 2011].

[14] Previous satellite data studies have identified correspondence of light, moderate, and heavy rain types

with warm rain/low clouds, mixed-phase rain/congestus, and ice-phase rain/high clouds, respectively [Lau and Wu, 2007, 2011; Masunaga and Kummerow, 2006]. Hence, the canonical global rainfall response to CO<sub>2</sub> warming captured in the CMIP5 model projection suggests a global scale readjustment involving changes in circulation and rainfall characteristics, including possible teleconnection of extremely heavy rain and droughts separated by far distances [Lau and Kim, 2012]. This adjustment is strongly constrained geographically by climatological rainfall pattern, and most likely by the GHG warming induced sea surface temperature anomalies [Xie et al., 2009] with unstable moister and warmer regions in the deep tropics getting more heavy rain, at the expense of nearby marginal convective zones in the tropics and stable dry zones in the subtropics. Our results are generally consistent with so-called “the rich-getting-richer, poor-getting-poorer” paradigm for precipitation response under global warming [Allan et al., 2010; Lau and Wu, 2011; Zhou et al., 2011; Chou and Neelin, 2004; Chou et al., 2009]. We add that the increase in aridity in marginally convective zones in the tropical land under global warming is analogous to a “the-middle-class-also-getting-poorer” scenario. Further, our results suggest that there should be changes in rainfall types and cloud structures associated with a global shift in the climate norms induced by CO<sub>2</sub> warming. Ongoing studies (papers in preparation) by the authors have confirmed the importance of forcing from global warming induced anomalous sea surface temperature and vertical motions in governing the canonical spatial pattern of the global rainfall response to CO<sub>2</sub> warming. Finally, we stress that while this work provides a unifying global perspective of rainfall response to CO<sub>2</sub> increase, more work is needed to unravel the rainfall response to climate forcing not only from CO<sub>2</sub> but also from other greenhouse gases, as well as also from local and regional forcing such as sea surface temperature, aerosols, land use change, and dynamical feedback processes.

[15] **Acknowledgments.** This work is partially funded by the Precipitation Measurement Missions (PMM) and the CMIP5 Diagnostic Project, Modeling and Analysis Program (MAP), NASA headquarters. K.-M. Kim was also supported by the Korea Meteorological Administration Research and Development Program under grant CATER 2012–2062.

[16] The Editor thanks two anonymous reviewers for their assistance in evaluating this paper.

## References

- Allan, R. P., B. J. Soden, V. O. John, W. Ingram, and P. Good (2010), Current changes in tropical precipitation, *Environ. Res. Lett.*, doi:10.1088/1748-9326/5/52/025205.
- Andrews, T., P. M. Forster, O. Boucher, N. Bellouin, and A. Jones (2010), Precipitation, radiative forcing and global temperature change, *Geophys. Res. Lett.*, 37, L14701, doi:10.1029/2010GL043991.
- Brubaker, K. L., and D. Entekhabi (1996), Analysis of feedback mechanisms in land-atmosphere interaction, *Water Resource Res.*, 32, 1343–1357.
- Chou, C., and J. D. Neelin (2004), Mechanisms of global warming impacts on regional tropical precipitation, *J. Climatol.*, 17, 2688–2701.
- Chou, C., J. D. Neelin, C. A. Chen, and J. Y. Tu (2009), Evaluating the “rich-get-richer” mechanism in tropical precipitation change under global warming, *J. Clim.*, 22, 1982–2005.
- Chou, C., C.-A. Chen, P.-H. Tan, and K.-T. Chen (2012), Mechanisms for global warming impacts on precipitation frequency and intensity, *J. Clim.*, 25, 3291–3306.
- Field, C. B., et al. Eds. (2012), Managing the risks of extreme events and disasters to advance climate change adaptation: special report of the intergovernmental panel on climate change. <http://ipcc-wg2.gov/SREX/>
- Frieler, K., M. Meinshausen, T. Schneider von Deimling, T. Andrews, and P. Forster (2011), Changes in global-mean precipitation in response to warming, greenhouse gas forcing and black carbon, *Geophys. Res. Lett.*, 38, L04702, doi:10.1029/2010GL045953.

- Giorgi, F., E. Coppola, E. S. Im, N. S. Diffenbaugh, X. Gao, and Y. Shi (2011), Higher hydroclimatic intensity with global warming, *J. Clim.*, 24, 5309–5324.
- Groisman, P. Y., R. W. Knight, D. R. Easterling, T. R. Karl, G. C. Hergel, and V. N. Razuvaev (2005), Trends in intense precipitation in the climate record, *J. Clim.*, 18, 1326–1350.
- Held, I. M., and B. J. Soden (2006), Robust responses of the hydrological cycle to global warming, *J. Climate*, 19, 5686–5699.
- Hu, Y., and Q. Fu (2007), Observed poleward expansion of the Hadley circulation since 1979, *Atmos. Chem. Phys.*, 7, 5229–5236.
- IPCC (2007), Climate change 2007: The physical science basis. Contribution of working group I to the fourth assessment report of the intergovernmental panel on climate change [Solomon, S., D. Qin, M. Manning, Z. Chen, M. Marquis, K.B. Averyt, M. Tignor and H.L. Miller (eds.)]. Cambridge University Press, Cambridge, United Kingdom and New York, NY, USA, 996 pp.
- Kharin, V., F. W. Zwiers, X. Zhang, and G. C. Hegerl (2007), Changes in temperature and precipitation extremes in IPCC ensemble of coupled model simulations, *J. Climate*, 20, 1419–1444, doi:10.1175/JCLI4066.1.
- Lau, K.-M., and K.-M. Kim (2012), The 2010 Pakistan flood and Russian heat wave: Teleconnection of hydrometeorologic extremes, *J. Hydromet.*, 13, 392–403.
- Lau, K. M., and H.-T. Wu (2007), Detecting trends in tropical rainfall characteristics, 1979–2003, *Int. J. Climatol.*, 27, 979–988.
- Lau, K.-M., and H.-T. Wu (2011), Climatological and changes in tropical oceanic rainfall characteristics inferred from Tropical Rainfall Measuring Mission (TRMM) data (1998–2009), *J. Geophys. Res.*, 116, D17111, doi:10.1029/2011JD015827.
- Lee, J.-E., B. R. Lintner, C. K. Boyce, and P. J. Lawrence (2011), Land use change exacerbates tropical South American drought by sea surface temperature variability, *Geophys. Res. Lett.*, 38, L19706, doi:10.1029/2011GL049066.
- Lintner, B. R., M. Biasutti, N. S. Diffenbaugh, J.-E. Lee, M. J. Niznik, and K. L. Findell (2012), Amplification of wet and dry month occurrence over tropical land regions in response to global warming, *J. Geophys. Res.*, 117, D11106, doi:10.1029/2012JD017499.
- Liu, C., R. P. Allan, and G. J. Huffman (2012), Co-variation of temperature and precipitation in CMIP5 models and satellite observations, *Geophys. Res. Lett.*, 39, L13803, doi:10.1029/2012GL052093.
- Masunaga, H., and C. D. Kummerow (2006), Observations of tropical precipitating clouds ranging from shallow to deep convective systems, *Geophys. Res. Lett.*, 33, L16805, doi: 10.1029/2006GL026547.
- Min, S.-K., X. Zhang, F. W. Zwiers, and G. C. Hegerl (2011), Human contribution to more intense precipitation extremes, *Nature*, 470, 378–381.
- O’Gorman, P. A., and T. Schneider (2009), The physical basis for increases in precipitation extremes in simulations of 21st-century climate change, *Proc. Natl. Acad. Sci. U. S. A.*, 106, 14773–14777.
- Riahi, K., S. Rao, V. Krey, C. Cho, V. Chirkov, G. Fischer, G. Kindermann, N. Nakicenovic, and P. Rafaj (2011), RCP 8.5—A scenario of comparatively high greenhouse gas emissions, *Clim. Chang.*, 109, 33–57.
- Scheffé, J., and D. M. Frierson (2012), Robust future precipitation declines in CMIP5 largely reflect the poleward expansion of model subtropical dry zones, *Geophys. Res. Lett.*, 39, L18704, doi:10.1029/2012GL052910.
- Seidel, D. J., Q. Fu, W. J. Randel, and T. J. Reichler (2008), Widening of the tropical belt in a changing climate, *Nat. Geosci.*, 1, 21–24.
- Sheffield, J., and E. F. Wood (2008), Projected changes in drought occurrence under global warming from multi-model, multi-scenario IPCC AR4 simulations, *Clim. Dyn.*, 31, 79–105.
- Sun, F., M. L. Roderick, and G. D. Farquhar (2012), Changes in the variability of global land precipitation, *Geophys. Res. Lett.*, 39, L19402, doi:10.1029/2012GL053369.
- Taylor, K. E., R. J. Stouffer, and G. A. Meehl (2012), An overview of CMIP5 and the experiment design, *Bull. Amer. Meteor. Soc.*, 93, 485–498.
- Trenberth, K. E. (2011), Changes in precipitation with climate change, *Clim. Res.*, 47, 123–138, doi:10.3354/cr00953.
- Trenberth, K. E., A. Dai, R. M. Rasmussen, and D. B. Parsons (2003), The changing character of precipitation, *Bull. Amer. Meteor. Soc.*, 84, 1205–1217.
- Vecchi, G. A., B. J. Soden, A. T. Wittenberg, I. M. Held, A. Leetmaa, and M. J. Harrison (2006), Weakening of tropical Pacific atmospheric circulation due to anthropogenic forcing, *Nature*, 441, 73–76.
- Xie, S. P., C. Deser, G. Vecchi, J. Ma, H. Teng, and A. Witterberg (2009), Global warming pattern formation: sea surface temperature and rainfall, *J. Clim.*, 23, doi:10.1175/2009JCLI3329.1.
- Yin, J. H. (2005), A consistent poleward shift of the storm tracks in simulations of 21st century climate, *Geophys. Res. Lett.*, 32, L18701, doi:10.1029/2005GL023684.
- Zhou, Y. P., K.-M. Xu, Y. C. Sud, and A. K. Betts (2011), Recent trends of the tropical hydrological cycle inferred from Global Precipitation Climatology Project and International Satellite Cloud Climatology Project data, *J. Geophys. Res.*, 116, D09101, doi:10.1029/2010JD015197.